

## **New perspectives on radium behavior within a subterranean estuary**

Meagan Eagle Gonneea<sup>1</sup>, Paul K. Morris<sup>2</sup>, Henrieta Dulaiova<sup>1</sup>, and Matthew A. Charette<sup>1</sup>

<sup>1</sup>Department of Marine Chemistry and Geochemistry, Woods Hole Oceanographic Institution, Woods Hole, MA, 02543 USA

<sup>2</sup>National Oceanography Centre, Southampton (NOCS), UK

### **Abstract:**

Over the past decade, radium isotopes have been frequently applied as tracers of submarine groundwater discharge (SGD). The unique radium signature of SGD is acquired within the subterranean estuary, a mixing zone between fresh groundwater and seawater in coastal aquifers, yet little is known about what controls Ra cycling in this system. The focus of this study was to examine controls on sediment and groundwater radium activities within permeable aquifer sands (Waquoit Bay, MA, USA) through a combination of field and laboratory studies. In the field, a series of sediment cores and corresponding groundwater profiles were collected for analysis of the four radium isotopes, as well as dissolved and sediment associated manganese, iron, and barium. We found that in addition to greater desorption at increasing salinity, radium was also closely tied to manganese and iron redox cycling within these sediments. A series of laboratory adsorption/desorption experiments helped elucidate the importance of 1) contact time between sediment and water, 2) salinity of water in contact with sediment, and 3) the chemical characteristics of sediment on radium adsorption/desorption. We found that these reactions are quick, on the order of hours, that desorption increases with salinity and that presence of Fe and Mn (hydr)oxides on the sediment inhibit the release of radium. These sediments have a large capacity to sorb radium from fresh water, and with Fe and Mn (hydr)oxide coatings, can sorb Ra from high salinity water. Combined with these experimental results, we present evidence from time series measurements that within this subterranean estuary there are cyclic periods of Ra accumulation and release controlled by changing salinity and redox conditions.

**Keywords:** radium; sediments; desorption; adsorption; barium; submarine groundwater discharge; subterranean estuary; redox reactions; ion exchange

## 1. Introduction

The subterranean estuary (STE), as defined by Moore (1999), is an underground chemically reactive zone of mixing between fresh groundwater and seawater that intrudes into the aquifer. Chemical reactions within this zone combined with submarine groundwater discharge (SGD) are known to have a large impact on coastal budgets of various constituents including nutrients, trace metals and radioisotopes (Charette and Sholkovitz, 2002; Windom and Niencheski, 2003; Slomp and van Cappellen, 2004). Many studies have utilized the unique geochemical signal originating from the subterranean estuary to determine rates of transport of such constituents to the coastal ocean via submarine groundwater discharge (see Burnett et al., 2006 and references therein). Examples of SGD tracers are the four naturally occurring radium isotopes ( $^{223}\text{Ra}$ ,  $^{224}\text{Ra}$ ,  $^{226}\text{Ra}$  and  $^{228}\text{Ra}$ ); their use in this approach is based on measuring the excess radium due to SGD, and the radium activity in the groundwater that supplied the excess. The latter parameter usually varies considerably, and is therefore one of the largest sources of uncertainty in Ra-derived SGD rates. In order to reduce this uncertainty, we require a better understanding of what controls Ra cycling in coastal groundwater systems.

Our perception of how Ra might behave in subterranean estuaries has mostly been derived from studies of their above-ground counterpart. Ra release in surface estuaries has been mainly attributed to desorption of Ra from suspended and bottom sediments as salinity increases (Li and Chan, 1979; Elsinger and Moore, 1980). Radium behavior within the STE has additional complexity. There are several potential geochemical controls on Ra activities within groundwater including bulk and exchangeable sediment Ra activities (Porcelli and Swarzenski, 2003); grain size and porosity of sediments (Webster et al., 1995, Hancock et al., 2006); changes in ionic strength (salinity) of groundwater (Elsinger and Moore, 1980; Webster et al., 1995); temperature effects (Rama and Moore, 1996) and barite solubility (barium (Ba) and Ra are chemical analogs) (Langmuir and Riese, 1985; Grundl and Cape, 2006). Other controls have been suggested but not thoroughly examined including the redox state of groundwater

(including Eh and pH) (Puigdomènech and Bergström, 1995; Porcelli and Swarzenski, 2003) and the presence of manganese (Mn) (hydr)oxides, since Ra has a very high affinity for Mn (Bollinger and Moore, 1993; Sun and Torgersen, 2001; Charette and Sholkovitz, 2006).

It is well known that sediment redox conditions drive the solubility of Mn and Fe, in particular that Mn and Fe are mobilized when both Eh and pH decrease (Miao et al., 2006). This potential control on Ra desorption has not been thoroughly explored due to the limited data on *in situ* groundwater redox chemistry coupled with groundwater and sediment radium activities. In addition, most laboratory work on Ra adsorption/desorption has not maintained *in situ* redox conditions.

There is also a paucity of *in situ* data on sediment Ra activities and resulting pore water Ra levels. Much of the data on sediment Ra activities are collected from discreet depths from wells and piezometers or consist of depth profiles for surface or shallow (<1 m) sediments. While important geochemical reactions do occur over this depth, there is likely additional complexity that will impact Ra cycling in deeper sediments. Due to the small number of data on Ra activities within STE sediments, particularly saturated sands, from depths greater than one meter, much of the Ra sediment chemistry is based on surface or shallow sediments and scaled to the larger study area.

This study investigates the sediment and groundwater radium distributions within the STE of Waquoit Bay. This system has been extensively studied, with a well established underground mixing zone between fresh groundwater and recirculating seawater occurring over a narrow (~10 m) region (Figure 1), creating an ideal natural laboratory for investigating sediment and groundwater Ra dynamics. Seasonal changes in water table height result in movement of the fresh/salt interface, thus periodically changing the ionic strength and redox conditions of the water saturating sediments. Recharge of the aquifer occurs during the winter and spring, and the fresh/salt interface moves seaward, while during the summer and fall, the aquifer levels drop and sea water intrudes further into the STE (Michael et al., 2005).

In addition, there are active Fe/Mn redox cycles within the Waquoit Bay STE sediments (Charette and Sholkovitz, 2002; Charette et al., 2005). Charette and Sholkovitz (2006) proposed several controls on Ra chemistry, including 1) adsorption onto Fe/Mn

(hydr)oxides, 2) desorption from sediments via ion-exchange reactions, 3) release from oxides undergoing reductive dissolution and 4) sediment weathering. Here we report on a series of sediment cores and groundwater profiles which were collected to examine Ra dynamics *in situ*. Additional information about the Fe/Mn redox cycles of the Waquoit Bay STE is presented for sediments deeper in the aquifer (7 m) so we can evaluate how *in situ* redox conditions affect Ra cycling in these sediments. Finally, a series of laboratory experiments were then carried out on the collected sediment to further explore adsorption/desorption reactions rates and sediment partition coefficients ( $K_d$ ) under varying ionic strength and for sediments of differing Mn and Fe (hydr)oxide content.

## **2. Methods**

### **2.1 Study Area**

Waquoit Bay is a shallow estuary located along the southern shore of Cape Cod, MA, USA (Figure 1). The upper 10 m of the Cape Cod aquifer consists of fairly homogenous permeable sediments (Cambareri and Eichner, 1998) with a well defined subterranean estuary beneath the shore of Waquoit Bay (Testa et al., 2002; Talbot et al., 2003; Michael et al., 2005). Numerous studies have documented the importance of submarine groundwater discharge on nutrient and chemical budgets in Waquoit Bay (Valiela, et al., 1990; Charette et al., 2001; Bone et al., 2006). Radium isotopes have been employed to determine the magnitude of SGD and several studies report considerable variability in groundwater radium activities (Charette et al., 2001; Abraham et al., 2003; Gonnee et al., 2006; Mulligan and Charette, 2006). Initial studies of the sediment geochemistry describe a zone of Fe hydr(oxide) coated sands resulting from the precipitation of oxides from a large Fe plume in the fresh groundwater (Charette and Sholkovitz, 2002). Charette et al. (2005) describes the redox chemistry of Fe, Mn, Ba, U and Th in the upper 2 m of the aquifer.

Samples for this study were collected in June 2006, when aquifer levels were dropping and the fresh/saline groundwater interface was moving landward, inundating sediments that had been exposed to freshwater during the winter recharge period of the aquifer with higher salinity groundwater.

### **2.2 Field Methods**

A series of three sediment cores (down to 7 m) were collected in June 2006 with a hand operated bailer boring auger system (Figure 1). The sediment was collected in the 60 cm long auger which was pushed into the ground and filled with sediment. The recovered sediment was then pulled up to the surface and collected in sample bags. As the auger was removed, a plastic core casing was pushed down the hole to prevent sand from collapsing into the hole. The theoretical sampling resolution is 60 cm, limited by the length of the sediment auger barrel; however in practice “heaving” sands at depth resulted in sediment from the depth of the bottom of the core casing being pushed up the casing. Sediments pushed up the core casing in this way were assigned a depth corresponding to the bottom of the core casing. A very distinct color stratigraphy associated with different Fe and Mn (hydr)oxide layers was observed in the sediments, which verifies that we successfully sampled distinct sediment depths.

Groundwater samples were collected concurrently with the sediment samples, at a site 1.5 m offset from the coring site. A hollow stainless steel drive point piezometer system (Retract-a-tip™) with a sampling resolution of 0.15 m was used (Charette and Allen, 2006). Water was pumped through a clean nylon tube within the piezometer with a peristaltic pump. Basic water chemistry data including salinity, dissolved oxygen, temperature, pH and ORP (standardized to Eh) was measured with a YSI 600XLM in a flow-through cell (YSI, Inc.) In addition, separate water samples were collected for salinity and were analyzed by a Guideline AutoSal instrument. Samples for trace metals were collected in pre-acidified (2 µL/ml 8 N Optima nitric acid) HDPE containers. Groundwater (4L) was filtered through MnO<sub>2</sub> impregnated acrylic fibers (hereafter Mn fibers) at a flow rate of 0.2 L/minute to quantitatively sorb Ra onto the MnO<sub>2</sub> (Moore and Reid, 1973).

### **2.3 Laboratory Methods**

Sediments were brought back to the laboratory and stored wet at 4°C prior to analysis. Subsamples from the three sediment cores were dried, sealed with epoxy resin and left for > 3 weeks to ensure secular equilibrium between <sup>226</sup>Ra and its daughter radionuclides and then counted on planar gamma detectors for bulk sediment <sup>228</sup>Ra and <sup>226</sup>Ra via <sup>228</sup>Ac at 338 keV and <sup>214</sup>Pb at 351.9 keV. Porosity and sediment bulk density were determined for each sample. Grain size was determined with a Beckman Coulter

LS13320 laser diffraction particle size analyzer. A portion of each sediment sample was subjected to an operationally defined leach to determine the concentrations of Fe, Mn, Th, Ba and U associated with amorphous and crystalline oxides of Fe and Mn (Hall et al., 1996). Briefly, 0.2 g of sediment was combined with 10 mL of 0.25 M hydroxylamine hydrochloride in 25% glacial acetic acid and heated for 3 hours at 90°, decanted and then the leaching was repeated. An aliquot of the leachate was diluted 1:50 with 1 N Optima grade nitric acid. The resulting solution was analyzed via inductively coupled mass spectrometry on a Finnigan Element high resolution ICP-MS at Woods Hole Oceanographic Institution. Indium (In) was used as an internal standard to account for instrument drift and matrix effects of the solution. Count rates for all elements were normalized to In measured in samples and standards.

The Mn fibers with the groundwater radium isotopes and sediment desorption Ra (Section 2.4) were partially dried and placed within a delayed coincidence counter to measure  $^{223}\text{Ra}$  and  $^{224}\text{Ra}$  (Moore and Arnold, 1996). Samples were then ashed (820°C, 16 h) and homogenized prior to being placed within a well-type gamma spectrometer to measure  $^{226}\text{Ra}$  and  $^{228}\text{Ra}$  (Charette et al., 2001). All detectors were standardized using a NIST-certified Standard Reference Material sorbed to Mn fibers and prepared in the same manner as the samples.  $^{223}\text{Ra}$ ,  $^{224}\text{Ra}$ , and  $^{228}\text{Ra}$  activities were decay corrected for the time of collection.

Groundwater concentrations of dissolved Fe, Mn, Ba, Sr and U were measured by ICP-MS as described above for sediment leach samples. Each sample was diluted 1:20 with 1 N Optima nitric acid and spiked with an internal In standard.

#### **2.4 Adsorption/desorption experiments**

The amount of exchangeable surface bound Ra associated with sediments was assessed with a series of experiments. Sediment from three depths in PZ 11 including 1) 2.1 to 3.1 m, 2) 4.5 to 5.6 m and 3) 5.8 to 6.5 m, referred to hereafter as the top, middle and bottom of the core respectively, were chosen based on their differing sediment chemistry and resulting coloration (see shaded areas in Figure 1 and Table 1). First, the amount of surface bound  $^{226}\text{Ra}$  was determined via radon emanation after the sediment had equilibrated with 500 ml of radium free water with a salinity of 10.8.

For the second experiment, multiple, sacrificial replicates of sediment were mixed with water of varying salinities and left for various time periods. 350 g wet weight of sediment was mixed in cubetainers with 4 L of Ra-free water, either salinity 5, 15 or 25, added to the sediment aliquots and left for 0.5, 2, 5, 10, 24 and 48 h. An additional experiment to test the time dependence of desorption was sampled at 288 and 4150 hours (at salinity 5 and 25 only). The samples were shaken twice, immediately after the water was added and 1 minute before the water was separated from the sediment by decanting it into another container. Decanted water was pumped sequentially through clean acrylic fiber and then Mn fiber at a rate of  $< 0.4 \text{ L min}^{-1}$ . The clean acrylic fiber served as a prefilter to remove the bulk of fine, suspended particles contained within the decanted sample and the Mn fiber was used to extract all the Ra that had been desorbed into the water. The Mn fiber was then rinsed with Ra-free fresh water to remove any salts from the fiber.

The third experiment was designed to ascertain total ion exchangeable Ra for these sediments. 100 dpm of  $^{226}\text{Ra}$  was spiked into 20 ml of Ra-free groundwater with a salinity of 0 or 25 and then dripped through sediment columns filled with ~15 grams dry weight of sediment at a flow rate of 6-8 ml/h. The solution was passed over the sediment twice, resulting in a total exposure time of 6 hours. The  $^{226}\text{Ra}$  was removed from solution by precipitation of  $\text{BaSO}_4$  (modified from Martin et al., 1995). The barite was sealed in a counting vial with epoxy and equilibrated for 3 weeks to allow for the ingrowth of  $^{214}\text{Pb}$  and  $^{226}\text{Ra}$  was determined by gamma spectrometry via  $^{214}\text{Pb}$  at 351.9 keV.

Groundwater of varying salinity was prepared for these experiments by mixing fresh groundwater with seawater. Fresh groundwater was collected from the Waquoit STE, and saline water was collected from Vineyard Sound, the seawater source to Waquoit Bay and ultimately the STE. The water was filtered ( $1 \mu\text{m}$ ) to remove the bulk of the particulates and then passed through Mn fibers to ensure the water used was free of Ra. The freshwater and seawater was then mixed in varying ratios until the desired salinity was achieved.

## **2.5 Time series data**

A series of permanent piezometer wells, similar to the field sampling system used above, was installed in 2004 and has been sampled at monthly intervals since. The wells

were installed at various depths to capture the extent of the fresh/saline interface as it rose and fell seasonally. The same suite of samples is collected from these wells as was collected during field sampling of groundwater, including salinity, Eh, trace metals, and radium, with the same methods employed to analyze these samples.

### **3. Results and Discussion**

The Waquoit Bay STE has a well-defined mixing zone between fresh groundwater and circulating seawater. In our study area, the mixing zone between these two components is narrow, usually occurring over 1-2 m, and rises toward the sediment surface to outcrop at approximately the low-tide line. Thus, landward piezometer profiles have a broad region of fresh groundwater, which gets progressively shallower in seaward profiles. There are three main salinity zones within these profiles, 1) the freshwater zone, 2) the salinity transition zone, where mixing between the fresh and saline water causes groundwater salinities to rise sharply from fresh to near 20, and 3) the circulating seawater zone, where salinity is greater than 20.

The redox conditions in the groundwater are closely tied to the salinity, since saline groundwater results from the intrusion of bay water that has passed through organic rich surface sediments. When this water enters the aquifer, the organic matter degrades along the flow path consuming dissolved oxygen, resulting in reducing conditions. In contrast, the fresh groundwater is relatively oxidized. Thus, increases in salinity related to recirculating seawater correspond to decreases in oxidation-reduction potential (Eh). Some small salinity increases at the top of the groundwater profiles do not correspond to decreases in Eh, likely because the salinity is due to “overtopping” of new bay water from a high tide that has not resided in the aquifer long enough to become significantly reducing. Within the three salinity zones described above, redox conditions can be either oxidizing (high Eh) or reducing (low Eh) depending on its associated organic matter content and how much time the water has spent within the aquifer.

There are four important redox-controlled zones within the sediment where Fe and Mn (hydr)oxides either accumulate on the sands in substantial levels or are released (Figure 3). 1) The top of all profiles are oxidizing, with high Eh values. There is some accumulation of sediment Mn (hydr)oxides (PZ 6 and 7) and Fe (hydr)oxides (PZ 6) within this zone. 2) A reducing zone follows which is associated with a small (1-2)

increase in salinity. This zone is marked by a release of Ra, Ba, Mn and Fe from the sediments. 3) A second oxidizing zone follows, which is marked by an accumulation of Fe (hydr)oxides above Mn (hydr)oxides. 4) Finally, associated with the circulating seawater, the reducing zone at the bottom of each profile is marked by a further release of Ra, Ba, Mn and Fe. A more detailed discussion of these phenomena follows.

### 3.1 Groundwater Chemistry

Three groundwater profiles (~8 m deep) were collected within the Waquoit STE to capture the extent of the mixing zone between fresh and saline water (Figure 1). PZ 7, the most landward, has a salinity of <2 from 1 to 3.5 m, then is fresh until salinity rises sharply to >10 at 7 m at the salinity transition zone (Figure 2). PZ 6 increases to a salinity of 1 at 5.5 to 6.4 m, then quickly becomes salty, reaching a maximum salinity of 21. PZ 11, the most seaward, increases to a salinity of 1 from 4.3 to 5.2 m, then increases to maximum salinity of 25 by 7.3 m (supplementary information Table 1).

Groundwater profiles show several zones of high Ra activity, usually one above the STZ within the predominantly fresh zone and one beginning concurrent with the STZ and continuing on through the saline zone.  $^{224}\text{Ra}$  (10 to 506 dpm/100L),  $^{223}\text{Ra}$  (0.5 to 30 dpm/100L),  $^{226}\text{Ra}$  (6 to 370 dpm/100L) and  $^{228}\text{Ra}$  (6-685 dpm/100L) activities within the STE range over two orders of magnitude (Figures 2 and 3).

The redox conditions of the water exhibit a strong control on dissolved Mn, Fe, Ba, and Ra (Figure 3). There are two zones of low Eh in each profile, an upper zone, 1-2 m thick located between 1 and 4 m depth associated with a plume of high dissolved Fe, and a lower one at the salinity transition zone in each profile. In all profiles, concurrent zones of low Eh and increased salinity are marked by increases in dissolved Ba, Mn, Fe and Ra, although the magnitude of increase in Ra is not always the same across all isotopes. For example, at 2 m in PZ 11, salinity rises to 1, Eh decreases, groundwater Ba increases from 15 to 300 nmol/kg, Mn from 0.2 to 6.9  $\mu\text{mol/kg}$ , Fe from 0.9 to 177  $\mu\text{mol/kg}$  and  $^{228}\text{Ra}$  from 18 to 120 dpm/100L.  $^{224}\text{Ra}$  (10 to 120 dpm/100L) and  $^{223}\text{Ra}$  (0.5 to 6.8 dpm/100L) also display peaks, but the  $^{226}\text{Ra}$  increase is much less pronounced (7 to 14 dpm/100L). There is a similar pattern at 1.5 m in PZ 6. This divergence in profiles

between the different isotopes is likely due the much longer half life of  $^{226}\text{Ra}$  resulting in a much longer regeneration time in the sediment.

It is important to note that in PZ 6 and PZ 11 there is an increase in Ba and Ra (all isotopes) in a highly oxidizing zone (4 m PZ 11, 5 m PZ 6). It seems likely that this release is due to ion exchange, since it occurs right at the beginning of the salinity transition zone. There is no concurrent increase in dissolved Mn or Fe, unlike in the reducing zone when Ba and Ra are mobilized. The release of Ba is linked to Ra cycling when both ion exchange and redox conditions affect desorption, while release of Mn and Fe concurrent with Ra release only occurs under reducing conditions. This pattern suggests that surface bound exchangeable Ra (and Ba) throughout the STE is weakly bound to sediments except in the presence of Mn and Fe (hydr)oxides, where Ra is strongly bound. Thus, the presence or absence of redox sensitive elements may provide insight into the mechanisms controlling radium adsorption/desorption.

### 3.2 Sediment Chemistry

Three sediment cores (5.5 to 7 m deep) were collected within the Waquoit STE concurrently with the groundwater profiles. There is no discernable pattern in the bulk sediment  $^{228}\text{Ra}$  ( $47 \pm 12$  dpm/100g) or  $^{226}\text{Ra}$  ( $39 \pm 6$  dpm/100g) profiles. The 228/226 for all sediments ranges from 0.7 to 1.7, with an average of 1.2 (supplementary information, Table 2).

Sediment-bound Mn (hydr)oxides have a distinct maxima at the bottom of each profile, peaking at  $>2000$   $\mu\text{mol/kg}$  in PZ 6 (7 m) and PZ 11 (6 m) and around  $1000$   $\mu\text{mol/kg}$  in PZ 7 (5m) (Figure 3, supplementary information Table 2). Sedimentary adsorbed Fe profiles are similar to Mn, however the Fe peak is above the Mn peak and is  $25,000$  to  $30,000$   $\mu\text{mol/kg}$  in PZ 6 (5 m) and PZ 11 (5 m) and around  $100,000$   $\mu\text{mol/kg}$  in PZ 7 (5 m). This Fe-rich zone was described as an “iron curtain” by Charette and Sholkovitz (2002), since it was shown to inhibit the transport into surface water of certain groundwater constituents (i.e. phosphate). The Mn (hydr)oxide-rich zone or “manganese curtain” likely serves as a barrier to the transport of certain elements, including Ba and Ra, which have a high affinity for Mn (hydr)oxides (40 times greater than Fe (hydr)oxides, Moore and Reid, 1973). Adsorbed Ba ranges from 0.5 to  $80$   $\mu\text{mol/kg}$  and

displays a distinct peak (2-8  $\mu\text{mol/kg}$ ) concurrent with the Mn (hydr)oxides. Within the Mn (hydr)oxide-rich zone, there is a linear relationship between sediment Mn and Ba, however no such relationship exists between sedimentary Fe and Ba. There is little variation in grain size (average 550 microns) or dry bulk density ( $2.6 \text{ g/cm}^3$ ) for sediments from any of the profiles. Porosity could not be determined directly on these sediments due to the manner of collection, which disturbed *in situ* conditions, so a published value of 25% was used (Cambareri and Eichner, 1998).

### 3.3 Desorption/Adsorption Experiments

For many of the processes that control Ra adsorption/desorption, it is useful to consider a model of a sediment grain with two fractions of Ra, a surface bound exchangeable fraction, whether it is bound to an organic coating, siliceous oxide or Mn-Fe (hydr)oxides, and the bulk sediment Ra, which includes Ra locked within the sediment is likely very different than the exchangeable fraction, particularly when coarse-grained sediments are present. These adsorption/desorption experiments were designed to provide information about the relative importance of a variety of parameters for Ra adsorption/desorption between the exchangeable pool on sediments and groundwater, including 1) length of exposure of sediments with water (time); 2) salinity of groundwater in contact with sediment; 3) exchangeable Ra content of sediment; 4) oxidized Mn and Fe precipitated on sediment. Temperature, another variable that affects Ra desorption (Rama and Moore, 1996), was held constant at  $17 \pm 0.8 \text{ C}$ . No attempt was made to maintain *in situ* redox conditions of the pore water, so these experiments are not appropriate to evaluate the influence of the redox state of the water on Ra desorption. These experiments were done with sediments from 1) the top of PZ 11 (inundated with freshwater, low sediment Mn and Fe), 2) middle of PZ 11 (inundated with water of salinity 1-5, within the “Fe curtain” with intermediate sediment Mn and high Fe) and 3) bottom of PZ 11 (inundated with water of salinity 17-23, within the “Mn curtain” with high sediment Mn and low Fe) (Table 1).

#### 3.3.1 Exchangeable Radium

The amount of surface bound  $^{226}\text{Ra}$  was determined via radon emanation and ranged from 6-32 dpm/100g  $^{226}\text{Ra}$  (20 to 70% of bulk) with considerably more surface bound/exchangeable  $^{226}\text{Ra}$  present at the bottom of PZ 11, within the “Mn curtain”, than elsewhere (Table 1). The pattern of exchangeable  $^{226}\text{Ra}$  enrichment in the bottom sediments compared to the upper sediments may be due in part to preferential removal of  $^{226}\text{Ra}$ , which has a much longer half-life than the other isotopes, from the upper 2 m of sediment, where there is increased flow (A. Mulligan, unpublished data). This pattern is also observed in the  $^{228}\text{Ra}/^{226}\text{Ra}$  ratio of groundwater, which decreases with depth.

### 3.3.2 Length of exposure

To determine the time dependence of Ra desorption, sediments were exposed to salinity 5 or 25 water for 0.2, 0.5, 1.5, 2.7, 5.2, 10, 25, 290 and 4150 hours. Samples at salinity 5 were run in duplicate and samples at salinity 25 in triplicate to evaluate natural variability, which is greater than analytical error. We looked at the slope of Ra desorbed versus hours of exposure and then did a simple statistical analysis (student t-test) to look at the variance two time periods, 0-25 and 200-4000 hours. There is no statistical difference (p value <0.05) between any of the time periods for  $^{226}\text{Ra}$  ( $0.58 \pm 0.14$  dpm/100g at salinity 5 and  $0.62 \pm 0.14$  dpm/100g at salinity 25) or  $^{228}\text{Ra}$  but  $^{223}\text{Ra}$  and  $^{224}\text{Ra}$  both increase with time.

The apparent difference in desorption between the long- and short-lived radium isotopes is due to the rate of radioactive ingrowth that occurs on the sediments for the duration of the experiments. Upon exposing the sediments with water, equilibrium between sorbed and dissolved radium is established with the dissolved state highly favored as ionic strength increases (high salinity~low sorption). As apparent from the long-lived radium results, the kinetics of this equilibrium is fast, on the order of minutes, as has been found elsewhere (Langmuir and Riese, 1985; Koulouris 1995). In case of the short-lived isotopes, radium is mobilized by recoil effects when it is continuously produced by the radioactive decay of its insoluble thorium parent so there is a continuous new supply of radium into the pore water. In case of the long-lived radium there is no new radium produced and only very minor concentration changes occur in the dissolved radium concentration.

Since samples were run in either duplicate or triplicate, we were able to determine the variability inherent in these desorption experiments. To do this, we compiled the standard deviation between duplicate or triplicate samples for each time point at each salinity. On average, the variance for  $^{224}\text{Ra}$  is 15%,  $^{223}\text{Ra}$  22%,  $^{226}\text{Ra}$  25% and  $^{228}\text{Ra}$  12% (with analytical error for these samples averaging:  $^{224}\text{Ra}$  4%,  $^{223}\text{Ra}$  16%,  $^{226}\text{Ra}$  10% and  $^{228}\text{Ra}$  6%). Given the large variance between duplicates/triplicates combined with the small increase in Ra desorbed over time, time of exposure has minimal impact on the amount of Ra desorbed, even for the short-lived isotopes which do display some increase with time. This result may be due in part to the experiment set-up, since after the water and sediment were mixed, no further shaking occurred until immediately prior to separating the water from the sediment. Thus, after the water immediately in contact with the sediments reached equilibrium with the sediments, diffusion was the main process to equilibrate the rest of the overlying water with the pore water.

Charette and Sholkovitz (2006) invoked a “slow weathering” hypothesis to explain the apparent continued input of Ba and Ra within the STE. They stated: “In contrast with the surface estuary, which continually receives “new” Ba through the transport of suspended particles, the particles that comprise a subterranean estuary are essentially static...thus, in a scenario where the sea level and aquifer recharge is relatively constant (hence, a relatively constant location of the groundwater-seawater mixing zone on decadal time scales), one would expect the desorptive input of Ba (and other alkaline earth elements) to be minimized. Only through the exposure of newly ion exchangeable Ba via slow weathering of aquifer minerals could this non-conservative release of Ba be maintained.” Our final time point from the desorption experiment was meant to test this hypothesis. Regardless of salinity, there is no measurable increase in the amount of  $^{226}\text{Ra}$  released from the sediment over ~6 months. Hence, we must invoke an alternative mechanism for explaining the apparent sustained input of Ba and long-lived Ra isotopes to STEs over time.

### 3.3.3 Salinity of groundwater

The effect of salinity on desorption was evaluated by exposing sediment to groundwater with a salinity of 5, 15 or 25 (Tables 1 and 2, Figure 4). As expected, there

is a significant increase in the amount of  $^{228}\text{Ra}$  and  $^{226}\text{Ra}$  desorbed at increasing salinities from 5 to 25 for all sediments. Since this decrease is mostly linear, here we discuss only salinity 25 and 5, with data provided for all salinities (Table 2). The percent increase in Ra that desorbs at salinity 25 compared to salinity 5 varied depending on which sediment was treated and which isotope was considered. 42% more  $^{228}\text{Ra}$  desorbs at salinity 25 from sediments from the top of PZ 11 (4.8 to 6.9 dpm/100g), but 80-131% more from sediments from the middle (0.35 to 0.81 dpm/100g) and bottom (0.41 to 0.74 dpm/100g) of PZ 11. 17-70% more  $^{226}\text{Ra}$  desorbs at salinity 25 from all PZ 11 sediments (top: 0.36 to 0.50; middle: 0.36 to 0.42; bottom: 1.24 to 2.11 dpm/100g). While most of the large increases in desorption are seen in sediments with low activities, thus are likely due in part to analytical uncertainty (i.e.  $^{228}\text{Ra}$  from the middle of PZ 11 had ~15% error), some occur in sediments with higher activities, such as  $^{226}\text{Ra}$  at the bottom of PZ 11 ( $^{226}\text{Ra}$  error <5%). Even with these large ranges in the increase in desorption from salinity 5 to 25 (from 17 to 131%), it is still apparent that increases in salinity do result in increased radium desorption, as has been previously observed (Elsinger and Moore, 1980; Webster et al., 1995). Given such a large range, it is difficult to give a percent increase in desorption that is applicable to all sediment types and Ra isotopes, however these increases cluster around a 50% increase in desorption from salinity 5 to 25 for these permeable siliceous sands. This value agrees with that of Webster et al. (1995), who reported a range from 0 to 66% increase in desorption between the same salinities for all four isotopes for sediment with a similar grain size from the Bega River.

### 3.3.4 Sediment chemistry and desorption

The sediments used for the desorption experiments were chosen based on their differing exchangeable Ra activities and Mn and Fe (hydr)oxide content (Table 1). In order to compare desorption from different sediments, we averaged the total Ra desorbed from all time points up to 48 hours for each isotope at each salinity (Table 2). There are several striking features of the desorption pattern of the different isotopes. The first is that sediments from the top desorb six times more  $^{228}\text{Ra}$  (4.8-6.9 dpm/100g) than sediments from the middle (0.35-0.81 dpm/100g, Fe curtain) and bottom (0.41-0.74 dpm/100 g, Mn curtain) of PZ 11. These sediments were from the freshwater portion of

the aquifer (at least at the time of collection), within the zone of high groundwater  $^{228}\text{Ra}/^{226}\text{Ra}$  ratios.

$^{226}\text{Ra}$  does not follow the same trend, with four times more desorbing from sediments in the “Mn curtain” at the bottom of PZ 11 (2500  $\mu\text{mol/kg}$  Mn and 43,000  $\mu\text{mol/kg}$  Fe). The top (45  $\mu\text{mol/kg}$  Mn and 8,700  $\mu\text{mol/kg}$  Fe) and middle (Fe-curtain, 1170  $\mu\text{mol/kg}$  Mn and 43,000  $\mu\text{mol/kg}$  Fe) of PZ 11 had very similar surface bound  $^{226}\text{Ra}$  activities (6-10 dpm/100g), while the bottom (Mn-curtain) sediment from PZ 11 had three times more exchangeable  $^{226}\text{Ra}$  (32 dpm/100g). Thus it appears, as expected, the presence of Mn (hydr)oxides is an important factor determining the total exchangeable Ra. Fe (hydr)oxides also likely play a role in sedimentary Ra dynamics at this location. Even though Ra has a 40 times lower affinity for Fe (hydr)oxides than Mn (hydr)oxides (Moore and Reid, 1973), sedimentary Fe is generally more abundant in these sediments than Mn. The Fe/Mn molar ratio for the top sediments is  $\sim 300$  and for the “Fe curtain” is  $\sim 40$ , while within the “Mn curtain” it is  $\sim 3.5$ .

### 3.3.5 $^{226}\text{Ra}$ adsorption

Ion exchangeable  $^{226}\text{Ra}$  was evaluated by passing 20 ml of groundwater with 100 dpm  $^{226}\text{Ra}$  through columns filled with separate aliquots of the same sediment used in the desorption experiments above. The results indicate that these sediments have a very large capacity to sorb  $^{226}\text{Ra}$ , up to 390 dpm/100g (Figure 5). Since the  $K_d$  of radium is known to decrease with increasing ionic strength, we predicted that much more  $^{226}\text{Ra}$  would adsorb onto sediments at 0 salinity than at 25 salinity. This is indeed the case for sediments from the top of PZ 11, where three times more radium adsorbs at 0 salinity (360 compared to 110 dpm/100g, Figure 5). However, within the “Fe curtain” and “Mn curtain” sediments, the difference between  $^{226}\text{Ra}$  adsorption at salinity 0 compared to salinity 25 is minimal. In sediments not coated with Mn and Fe (hydr)oxides, ion exchange is the primary mechanism for partitioning Ra between liquid and solid phases, where Ra is often physically bound. However, since Ra forms a chemical bond with Mn and Fe (hydr)oxides, the ionic strength of the solution does not greatly impact the amount of Ra that can be adsorbed onto the sediments. The evidence that Ra sorbs so efficiently at low salinities to all sediments and at high salinities to sediments coated with Mn and

Fe (hydr)oxides, provides a mechanism for concentrating Ra within the STE prior to episodic release events, such as the seasonal, landward shift in the fresh-saline groundwater interface.

### 3.3.5 Distribution coefficients

The distribution of radionuclides, including Ra, between sediment and water can be modeled with the sorption distribution coefficient ( $K_d$ ), which is defined here as the ratio of Ra in the solid phase (dpm/Kg) to Ra in the liquid phase in equilibrium with this sediment (dpm/L) and has units of L/Kg.

$$1) \quad K_d = Ra_{\text{solid}}/Ra_{\text{liquid}}$$

Distribution coefficients are determined in a variety of ways, usually in laboratory experiments where much greater than natural activities of a Ra isotope are spiked onto sediments (Rama and Moore, 1996; Hancock et al., 2006) or in laboratory experiments where sediment and water are equilibrated (Webster et al., 1995). In these cases,  $K_d$  only represents the distribution of radionuclides and does not ascertain what the main mechanisms of adsorption are. The assumption that thermodynamic equilibrium has been achieved is not valid for most *in situ* field conditions, since these systems are dynamic and include flowing groundwater. However, since these Ra adsorption/desorption reactions are fast, it is useful to compare *in situ* sediment and groundwater Ra activities ratios to laboratory determined  $K_d$  values.

Several caveats need to be identified to compare  $K_d$ s from various laboratory experiments to *in situ* sediment to groundwater Ra ratios since it is possible to control variables in experimental determinations of  $K_d$  but in the field, sediment characteristics, salinity and groundwater redox potential all vary simultaneously. One major difference with the laboratory experiments is the high water to sediment ratio (~5-30), resulting in an operationally defined  $K_d$  (based on the volume of water mixed with the sediment) that may be different than that expected in nature (Benes, 1990). It is also important to determine which fraction of the sedimentary Ra pool is being used to calculate  $K_d$ . In some instances, bulk sediment Ra is used, in others some operationally defined “exchangeable” fraction is used, the rationale being that Ra within the crystalline lattice of the sediment is not readily exchangeable with pore waters (Puigdomènech and

Bergström, 1995). This can, however, result in greatly differing  $K_d$  values. For example, if only 20% of total Ra in a sediment is defined as adsorbable or exchangeable, as we see within this STE, then the  $K_d$  would be much higher if the bulk Ra fraction were used in the  $K_d$  calculation. Here we determined exchangeable  $^{226}\text{Ra}$  via Rn-emanation for the three sediments from PZ 11, so for these experiments,  $K_d$  is reported using “exchangeable  $^{226}\text{Ra}$ .” We also calculated *in situ* sediment/groundwater Ra ratios for these sediments using groundwater collected from the same depth range as the sediments.

The desorption experiment  $K_d$  varies from 200 to 460, and decreases with increasing salinity (Table 3, Figure 6a). However, this relationship varies depending on the sediment type. The  $K_d$  decrease, for all three sediments, from salinity 5 to 25 is 16-40%. The salinity/  $K_d$  relationship can be described by a linear fit to the data:

- 2)  $K_d = -3.8 \times \text{salinity} + 480$  (Top),  $r^2 = 0.28$
- 3)  $K_d = -7.9 \times \text{salinity} + 425$  (Middle),  $r^2 = 0.05$
- 4)  $K_d = -3.0 \times \text{salinity} + 270$  (Bottom),  $r^2 = 0.57$

The presence of Mn and Fe (hydr)oxides has a greater impact on  $K_d$  than does an increase in salinity. Ra was strongly bound to sediments with greater amounts of Mn and Fe (hydr)oxides, although this relationship cannot be modeled with one linear fit (Figures 6b and 6c). When plotted against sediment Mn (hydr)oxide, there is a reduction in  $K_d$  with decreasing Mn (hydr)oxide content (Figure 6b). For “Fe curtain” sediments it is 43-53%. This fit a linear relationship:

- 5)  $K_d = 0.18 \times \text{sediment Mn } (\mu\text{mol/kg}) + 215$ ,  $r^2 = 0.66$

For “Mn curtain” sediments this relationship is:

- 6)  $K_d = 0.034 \times \text{sediment Mn } (\mu\text{mol/kg}) + 220$ ,  $r^2 = 0.25$

When the same  $K_d$ 's are plotted versus sediment Fe (hydr)oxides (Figure 6c), the relationship can be modeled with:

- 7)  $K_d = 0.0049 \times \text{sediment Fe } (\mu\text{mol/kg}) + 210$ ,  $r^2 = 0.38$

Thus, the presence of Mn and Fe (hydr)oxides has a greater impact on  $K_d$  than does an increase in salinity. For example, an increase in salinity from 5 to 15 results in a  $K_d$  decrease of only 50, while a  $K_d$  decrease of 200 can be attributed to a decrease in Mn (hydr)oxide content from ~1200 to 43  $\mu\text{mol/kg}$ .

Within the Waquoit STE, *in situ* ratios of sediment  $^{226}\text{Ra}$  to groundwater  $^{226}\text{Ra}$  vary from 90 to 1100 for the region where sediment for the above experiments was collected from (see shaded regions in Figure 3c). There is a decrease in the  $^{226}\text{Ra}$  sediment to groundwater ratio with increasing salinity, which is expected given the  $K_d$ :salinity relationship reported above (Figure 7a). Likewise, the  $^{226}\text{Ra}$  sediment to groundwater ratio also increases with increasing sedimentary Fe (hydr)oxide content (Figure 7c). The  $^{226}\text{Ra}$  sediment to groundwater ratio does increase with increasing sedimentary Mn (hydr)oxide content, as with the previous relationship established between the experimental  $K_d$  and Mn (hydr)oxide, however the relationship is specific to the sediment zone and not all sediments fit along the same line (Figure 7b). The sediments from the “Mn curtain” have the lowest  $^{226}\text{Ra}$  sediment to groundwater ratio, which is due to the dissolution of Mn (hydr)oxide, as evidence by high pore water dissolved Mn, and subsequent release of radium within this reducing zone, as seen in Figure 3c. Thus, it seems that the relationship between the *in situ*  $^{226}\text{Ra}$  sediment to groundwater ratio and sedimentary Mn (hydr)oxide content is driven by the pore water redox potential.

Previous estimates of the distribution coefficient for Ra range from 50 to 5000 (Puigdomènech and Bergström, 1995) (Table 4). Li and Chan (1979) reported a  $K_d$  of 235 for fine-grained Hudson Bay sediments. Webster et al. (1995) used a series of desorption experiments to construct a model of the effect of salinity on Ra desorption, and reported a  $K_d$  of 75 for fine-grained sediments. Rama and Moore (1996) reported a very low  $K_d$  of 45 (converted from 10 L/cm<sup>3</sup>) for fine-grained sediments from a salt marsh, and hypothesized that it was due to organic coating of the sediments, which neutralized the sorption capacity of the (Fe and Mn) mineral phases. The  $K_d$  values reported here from laboratory experiments, ranging from 200 to 460, are mostly higher than those reported for fine-grained sediments, as expected for permeable sands, but are in range with distribution coefficients of Ra in aquifers. The *in situ* sediment to groundwater Ra ratios display a greater range, from 90 to 1100, but also fall within the range of previously reported partitioning relationships.

#### 4. Conclusions

The adsorption/desorption experiments reveal several important characteristics of Ra behavior during sediment-water interaction in coastal aquifers. First, the length of time sediments are in contact with water does not significantly increase the amount of long-lived Ra that desorbs, verifying the conclusion of Langmuir and Riese (1985) that Ra adsorption-desorption reactions “go to completion within seconds to a few hours.” For modeling and other considerations, we can assume that groundwater radium is in equilibrium with the sediment. Second, increases in salinity result in more Ra desorbed, however the decrease in  $K_d$  associated with an increase in salinity varies depending on the chemical characteristics of the sediment. Sediments with greater amounts of Fe and Mn (hydr)oxides retain a greater proportion of Ra even when exposed to saline water, as is evident by the increase in  $K_d$  with increasing oxide content. In all, these sediments have a large capacity to sorb Ra, which is favored under low salinity conditions unless the sediment has significant amounts of Fe and Mn (hydr)oxides.

All these points were confirmed by a combination of *in situ* and laboratory experiments. Because the STE sediments are in a dynamic setting with flowing groundwater, the *in situ* derived  $K_{ds}$  are only valid if equilibrium states are established very quickly. The disadvantage of the laboratory experiments on the other hand is that it is hard simulate *in situ* pore water to sediment ratios and redox potentials.

The results from our laboratory experiments are supported by what we observe in the natural environment. The groundwater and sediment profiles within the Waquoit Bay STE indicate that salinity together with the Mn and Fe redox cycle all influence Ra partitioning. While radium has a much greater affinity for Mn (hydr)oxides than Fe (hydr)oxides, throughout much of the STE, Fe (hydr)oxides are more abundant than Mn (hydr)oxides (Fe/Mn ~ 40-300), thus both are likely involved in controlling sediment-water Ra partitioning. Though Ra desorption by ion exchange is an important process, it is difficult to decouple its importance relative to Fe and Mn within this STE, as the redox state is largely driven by the influx of organic matter carried by circulating seawater. Though salinity may be less effective than Fe and Mn redox chemistry at controlling Ra cycling in coastal groundwater systems, one must put into perspective the relative areas and concentrations over which these processes are at work in the STE. In our site, they

appear to be about equal but this may not be true in other STEs, given the large Fe and Mn (hydr)oxide content and vertical extent of the Waquoit aquifer sands.

To further evaluate the influence of redox conditions and salinity increases on radium within the STE, we looked at a time series of salinity, Eh, radium and metal concentrations at two depths within the STE. This approach has the advantage that we are evaluating the influence of changing salinity and redox conditions on a region of sediment within the aquifer. At 3.4 m, baseline salinity is <0.5, with increases of 1-2 seen twice in the record (Figure 8). At 4.7 m, baseline salinity is 25, with a decrease in salinity observed once. There are two release events of  $^{226}\text{Ra}$  (not including high value at beginning of time series), most visible at 3.4 m, where activities in the groundwater increase from a baseline of 4 dpm/100L to 80 to 170 dpm/100L. The first release event, between 8/05 and 11/05, is associated with an increase in salinity at 3.4 m to ~2. There is no associated decrease in Eh, and no release of Mn, although there is release of Ba, from 300 to 2240 nmol/L. The second release event, in 5/06 and 6/06, is associated with a rise in salinity at both depths and a decrease in Eh, which does not occur, however, until the second month of Ra release. There is a release of Mn at both depths and a release of Ba at 3.4 m. The Ra release at depth is much smaller since these sediments are continually inundated with saline water. The release of  $^{226}\text{Ra}$  at 3.4 m in 5/06 is about twice as great (170 dpm/100L) as the one observed between 8/05 and 11/05 (80 dpm/100L), yet the salinity increase at this time was less (1 rather than 2). While not conclusive, this suggests that the reducing conditions associated with the second Ra release play an important part in the magnitude of the release. These data provide *in situ* evidence that redox conditions are as important in Ra cycling as changes in groundwater salinity.

The seasonal shift in Ra derived from SGD as reported by Kelly and Moran (2002) and Charette (2007) require an annually renewable source of Ra within the STE. The long time scale (~6 month) desorption experiments reported here show that slow weathering cannot account for such an accumulation of Ra in coastal groundwater and subsequent flux to surface water via SGD. As shown here with adsorption experiments, these sediments have a large capacity to sorb Ra, particularly in fresh water. Using the above data, we calculated a simple radium balance between the low salinity period (when Ra sorbs to sediment, 200 days from 1/05 to 7/05) and higher salinity Ra release (60 days

from 8/05 to 11/05). During this period, there is 65 dpm/100 L addition to the sediment-groundwater system, as sorption onto sediments, while 90 dpm/100 L is lost as dissolution from sediments. Over 70% of the radium lost from the system can be accounted for by inputs when the sediment is inundated with fresh groundwater, thus providing an important mechanism to explain seasonal releases of radium within this STE. Moore (1997) hypothesized that a similar process was at work for the Ganges-Brahmaputra River delta. He suggested that during high river flow periods, the coastal aquifer within the delta region is recharged with freshwater, which loses its radium via sorption to sediments. Then, during low flow periods, saline water is allowed to enter the estuary and intrude into the river delta aquifer, where Ra is released via ion exchange driven desorption. This Ra-enriched fluid would then be carried to the coastal sea via SGD. While the overall mechanisms of Ra uptake/release are the same, the Waquoit STE is different in that the seasonal changes in aquifer height drive movement of the fresh/saline interface, a process that is independent of the salinity condition within the bay.

Given these findings, we recommend that future studies using Ra to derive SGD consider the following: 1) Ra activities should be measured across the full extent of the salinity range present in the groundwater. We observed Ra values at salinities of 1 and 25 that had the same activity. In addition, at salinities  $<1$ , we observed measurable radium, hence even “fresh” groundwater may be a source of radium to surface waters, especially when fresh groundwater represents a significant portion of total SGD (as in Mulligan and Charette, 2006). 2) Measure the groundwater and (if possible) sediment Mn and Fe content to determine if active cycling of these elements is present within the STE, since they influence Ra cycling. In the absence of Fe and Mn concentrations, groundwater redox potential (as measured by a YSI electrode or the equivalent) will provide useful information about the potential for active Fe and Mn redox cycling to be occurring. 3) If possible, determine exchangeable Ra inventories for sediment throughout the STE, since as we observed here, this value can vary considerably, even when bulk Ra shows little change. We recommend a simple approach for determining this quantity using  $^{222}\text{Rn}$  equilibration. 4) We observed seasonality in radium release within these sediments, thus measurements of groundwater radium activities collected in

one season may not be applicable to all seasons. Thus, groundwater radium activities should be determined concurrently with surface water measurements. Such measures should help insure the most appropriate groundwater radium activity is used, and thus minimizing associated uncertainty in calculations.

### **Acknowledgements**

The authors thank Paul Henderson, Gillian Smith, and DeAnna McCadney for assistance in the field and laboratory. David Schneider of the WHOI ICP-MS Facility performed the trace metal analyses. We extend our continued appreciation to the director and staff of the Waquoit Bay National Estuarine Research Reserve for their assistance with logistics during field sampling. This work is a result of research sponsored by NSF (OCE- 0425061 to M.A.C.), the WHOI-Southampton Graduate Student Exchange program, and the WHOI Postdoctoral Scholar program (to H.D.).

### **References**

- Abraham, D.M., Charette, M.A., Allen, M.C., Rago, A. and Kroeger, K.D., 2003. Radiochemical estimates of submarine groundwater discharge to Waquoit Bay, Massachusetts. *Biol. Bull.*, 205:246-247.
- Benes, P., 1990. Radium in continental surface water. In: IAEA Technical Report Series No. 310, *The Environmental Behaviour of Radium*, 1:373-418.
- Bollinger, M.S. and Moore, W.S., 1993. Evaluation of salt marsh hydrology using radium as a tracer. *Geochim. Cosmochim. Acta*, 57:2203-2212.
- Bone, S.E., Gonnessa, M.E. and Charette, M.A., 2006. Geochemical cycling of arsenic in a coastal aquifer. *Environ. Sci. Technol.*, 40:3273-3278.
- Burnett, W.C., Coward, J.B. and Deetae, S. 1990. Radium in the Suwannee River and estuary. *Biogeochem.* 10:237-255.
- Burnett, W.C., P.K. Aggarwal, A. Aureli, H. Bokuniewicz, J.E. Cable, M.A. Charette, E. Kontar, S. Krupa, K.M. Kulkarni, A. Loveless, W.S. Moore, J.A. Oberdorfer, J. Oliveira, N. Ozyurt, P. Povinec, A.M.G. Privitera, R. Rajar, R.T. Ramessur, J. Scholten, T. Stieglitz, M. Taniguchi, J.V. Turner, 2006. Quantifying submarine groundwater discharge in the coastal zone via multiple methods. *Sci. Total Environ.*, 367:498-543.
- Cambareri, T.C., and Eichner, E.M., 1998. Watershed delineation and ground water discharge to a coastal embayment. *Ground Water*, 36:626-634.
- Charette, M.A., Buesseler, K.O. and Andrews, J.E., 2001. Utility of radium isotopes for evaluating the input and transport of groundwater-derived nitrogen to a Cape Cod estuary. *Limnol. Oceanogr.*, 46:465-470.

- Charette, M.A. and Sholkovitz, E.R., 2002. Oxidative precipitation of groundwater-derived ferrous iron in the subterranean estuary of a coastal bay. *Geophys. Res. Lett.*, 29:1444-1447, doi: 10.1029/2001GL014512.
- Charette, M.A., Sholkovitz, E.R. and Hansel, C., 2005. Trace element cycling in a subterranean estuary: Part 1. Geochemistry of the permeable sediments. *Geochim. Cosmochim. Acta*, 69:2095-2109.
- Charette, M.A., and Allen, M.C., 2006. Precision ground water sampling in coastal aquifers using a direct-push, shielded-screen well-point system. *Ground Water Monit. R.*, 26(2):87-93.
- Charette, M.A., 2007. Hydrologic forcing of submarine groundwater discharge: Insight from a seasonal study of radium isotopes in a groundwater-dominated salt marsh estuary. *Limnol. Oceanogr.*, in press.
- Charette, M.A. and Shokovitz, E.R., 2006. Trace element cycling in a subterranean eastury: Part 2. Geochemistry of the pore water. *Geochim. Cosmochim. Acta*, 70:811-826.
- Elsinger, R.J. and Moore, W.S., 1980.  $^{226}\text{Ra}$  behavior in the Pee Dee River-Winyah Bay Estuary. *Earth Planet. Sc. Lett.*, 48:239-249.
- Gonneea, M. E., Mulligan, A. and Charette, M. A., 2006. Seasonal trends in radium activities within the mixing zone of a subterranean estuary, Waquoit Bay, MA. *Eos Transactions AGU Ocean Sciences Meeting Supplement*, 87(36), Abstract OS15B-01.
- Grundl, T. and Cape, M., 2006. Geochemical factors controlling radium activity in a sandstone aquifer. *Groundwater*, 44:518-527.
- Hall, G.E.M., Vaive, J.E, Beer, R. and Hoashi, M., 1996. Selective leaches revisited, with emphasis on the amorphous Fe oxyhydroxide phase extraction. *J. Geochem. Explor.*, 56:59-78.
- Hancock, G. J., Webster, I. T. and Stieglitz, T. C., 2006. Horizontal mixing of Great Barrier Reef waters: Offshore diffusivity determined from radium isotope distribution, *J. Geophys. Res.*, 111:C12019, doi:10.1029/2006JC003608.
- Kelly, R.P. and Moran S.B., 2002. Seasonal changes in groundwater input to a well-mixed estuary estimated using radium isotopes and implications for coastal nutrient budgets. *Limnol. Oceanogr.*, 47:1796-1807.
- Koulouris, G., 1995. Dynamic studies on sorption characteristics of  $^{226}\text{Ra}$  on manganese dioxide. *J. Radioan. Nucl. Ch. Ar.*, 193:269-279.
- Langmuir, D. and Riese, A.C., 1985. The thermodynamic properties of radium. *Geochim. Cosmochim. Acta*, 49:1593-1601.
- Li, Y. and Chan, L., 1979. Desorption of Ba and  $^{226}\text{Ra}$  from river-borne sediments in the Hudson estuary. *Earth Planet. Sc. Lett.*, 43:343-350.
- Martin, P., Hancock, G.J., Paulka, S. and Akber, R.A., 1995. Determination of  $^{227}\text{Ac}$  by  $\alpha$ -particle spectrometry. *Appl. Radiat. Isot.* 46:1065-1070.
- Miao, S, DeLaune, R.D. and Jugsujinda, A., 2006. Influence of sediment redox conditions on release/solubility of metals and nutrients in a Louisiana Mississippi River deltaic plain freshwater lake. *Sci. Total Environ.*, 371:334-343.
- Michael, H.A., Mulligan, A.E. and Harvey, C.F., 2005. Seasonal oscillations in water exchange between aquifers and the coastal ocean. *Nature*, 436:1145-1148.

- Moore, W.S., and Reid, D.F., 1973. Extraction of radium from natural waters using manganese-impregnated acrylic fibers. *J. Geophys. Res.*, 90: 6983-6994.
- Moore, W.S., and Arnold, R., 1996. Measurement of  $^{223}\text{Ra}$  and  $^{224}\text{Ra}$  in coastal water using a delayed coincidence counter. *J. Geophys. Res.*, 101: 1321-1329.
- Moore, W.S. 1997. High fluxes of radium and barium from the mouth of the Ganges-Brahmaputra River during low river discharge suggest a large groundwater source. *Earth Planet. Sc. Lett.*, 150:141-150.
- Moore, W.S., 1999. The subterranean estuary: a reaction zone of ground water and sea water. *Mar. Chem.*, 65:111-125.
- Mulligan, A.E., and Charette, M.A., 2006. Intercomparison of submarine groundwater discharge estimates from a sandy unconfined aquifer. *J. Hydrol.*, 327:411-425.
- Porcelli, D. and Swarzenski, P.W., 2003. The behaviour of U- and Th-series nuclides in groundwater. *Rev. Mineral. Geochem.*, 52:317-361.
- Puigdomènech and Bergström, U., 1995. Calculation of distribution coefficients for radionuclides in soils and sediments. *Nucl. Safety*, 36:142-154.
- Rama and Moore, W.S., 1996. Using the radium quartet for evaluating groundwater input and water exchange in salt marshes. *Geochim. Cosmochim. Acta*, 60:4645-4652.
- Slomp, C.P. and van Cappellan, P., 2004. Nutrient inputs to the coastal ocean through submarine groundwater discharge: controls and potential impact. *J. of Hydrol.*, 295: 64-86.
- Sun, Y. and Torgersen, T., 2001. Adsorption-desorption reactions and bioturbation transport of  $^{224}\text{Ra}$  in marine sediments: a one-dimensional model with applications. *Mar. Chem.*, 74:227-243.
- Talbot, J.M., Kroeger, K.D., Rago, A., Allen, M.C. and Charette, M.A., 2003. Nitrogen flux and speciation through the subterranean estuary of Waquoit Bay, Massachusetts. *Biol. Bull.* 205:244-245.
- Testa, J.M., Charette, M.A., Sholkovitz, E.R., Allen, M.C., Rago, A. and Herbold, C.W., 2002. Dissolved iron cycling in the subterranean estuary of a coastal bay: Waquoit Bay, Massachusetts. *Biol. Bull.* 203:255-256.
- Valiela, I., Costa, J., Foreman, K., Teal, J.M., Howes, B. and Aubrey D., 1990. Transport of Groundwater-Borne Nutrients from Watersheds and Their Effects on Coastal Waters. *Biogeochem.*, 10:177-197.
- Webster, I.T., Hancock, G.J., and Murray, A.S., 1995. Modeling the effect of salinity on radium desorption from sediments. *Geochim. Cosmochim. Acta*, 59:2469-2476.
- Windom, H. and Niencheski, F. 2003. Biogeochemical processes in a freshwater-seawater mixing zone in permeable sediments along the coast of Southern Brazil. *Mar. Chem.*, 83:121-130.

Sediment	Bulk $^{226}\text{Ra}$ dpm/100g	Desorbable $^{226}\text{Ra}^1$ dpm/100g	% Desorbable $^{226}\text{Ra}$ of bulk $^{226}\text{Ra}$	Bulk $^{228}\text{Ra}$ dpm/100g	Sediment $\text{Fe}^2$ $\mu\text{mol/kg}$	Sediment $\text{Mn}^2$ $\mu\text{mol/kg}$	Sediment 228/226
Top PZ 11, 2.1- 3.1 m	32 ± 1.1	6	19%	53 ± 2.8	13000	45	1.66
Middle, PZ 11, 4.6-5.6 m	38 ± 1.2	10	26%	44 ± 3.1	43000	1170	1.14
Bottom, PZ 11, 5.8-6.5 m	46 ± 1.3	32	70%	42 ± 2.8	8700	2500	0.90

<sup>1</sup>Desorbable  $^{226}\text{Ra}$  was determined via radon emanation after the sediment had equilibrated with salinity 10.8 water.

<sup>2</sup>Exchangeable Fe and Mn (hydr)oxides determined by leaching sediment in 0.25 M hydroxylamine hydrochloride in 25% glacial acetic acid and heated for 3 hours at 90°

Sediment	$^{226}\text{Ra}$ dpm/100g	$^{228}\text{Ra}$ dpm/100g	228/226
Top PZ 11, 2.1- 3.1 m	0.36/0.46/0.50	4.8/6.9/6.9	13/15/13
Middle, PZ 11, 4.6-5.6 m	0.36/.36/0.42	0.35/0.65/0.81	1/2/2
Bottom, PZ 11, 5.8-6.5 m	1.24/1.44/2.11	0.41/0.55/0.74	0.33/0.38/0.35

<sup>1</sup>Values are the average of all desorption values from 0 to 48 hours.

Salinity	Top PZ 11, 2.1-3.1 m	Middle, PZ 11, 4.6- 5.6 m	Bottom, PZ 11, 5.8- 6.5 m
5	260	460	380
15	210	430	330
25	200	390	220

<b>Table 4. Radium <math>K_d</math> values (L/Kg)</b>		
Aquifers	50 to 5000	Puigdomènech and Bergström (1995)
Fine-grained sediment Saline/fresh	235/21,000	Li and Chan (1979)
Fine-grained sediment	75	Webster et al. (1995)
Fine-grained sediment	45	Rama and Moore (1996)
Permeable sands	200-460	This Study

### Figure Captions

Figure 1: Waquoit Bay subterranean estuary sampling locations. The salinity transition zone (STZ) is indicated with a dashed line. The location of sediment and groundwater samples is marked by PZ 7, 6 and 11. Time series data comes from the TS profile. The shaded region indicates where sediment for the adsorption/desorption experiments was collected.

Figure 2: Groundwater  $^{224}\text{Ra}$  and  $^{223}\text{Ra}$  distributions at a) PZ 7, b) PZ 6 and c) PZ 11.

Salinity is the solid line in the first plot. Note the different scales for each isotope in each profile.

Figure 3: Groundwater profiles of salinity, Eh,  $^{226}\text{Ra}$ ,  $^{228}\text{Ra}$ , Ba and Mn and sediment Mn and Fe for a) PZ 7, b) PZ 6 and c) PZ 11. Shaded regions indicate where sediment for the adsorption/desorption experiments was collected. Note the different scales for each profile.

Figure 4: Desorbed radium from PZ 11 top (gray squares), PZ 11 middle (black triangles) and PZ 11 bottom (empty circles) at a)  $^{228}\text{Ra}$  at salinity 5, b)  $^{226}\text{Ra}$  at salinity 5, c)  $^{228}\text{Ra}$  at salinity 25 and d)  $^{226}\text{Ra}$  at salinity 25.

Figure 5: A plot of the adsorption of  $^{226}\text{Ra}$  on various types of sands against salinity.

Figure 6: Experimental distribution coefficients ( $K_d$ ) plotted against a) salinity, b) sediment Mn (hydr)oxides and c) Fe (hydr)oxides. The linear fits between  $K_d$  and salinity in a) are represented by the dotted line (top), dashed line (middle) and solid line (bottom). The linear fit between sediment Mn (hydr)oxides and  $K_d$  in b) are represented by the solid line (between top and middle) and dashed line (between top and bottom). The solid line in c) represents the fit for all sediment Fe (hydr)oxides and  $K_d$ .

Figure 7: *In situ*  $^{226}\text{Ra}$  sediment to groundwater ratios plotted against a) salinity, b) sediment Mn (hydr)oxides and c) Fe (hydr)oxides.

Figure 8: Time series measurements at 3.4 m (open symbols) and 4.7 m (filled symbols) within the Waquoit Bay STE of a) salinity, b) Eh, c)  $^{226}\text{Ra}$ , d) dissolved Mn and e) dissolved Ba. Note the different scales for the parameters between the two depths.

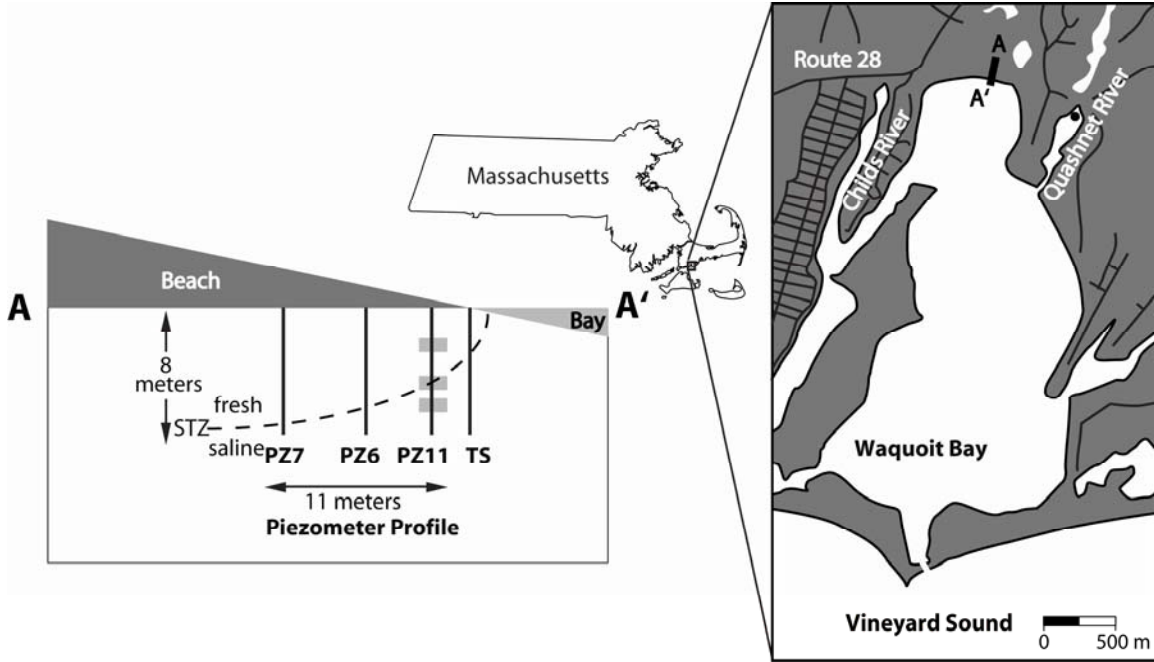


Figure 1

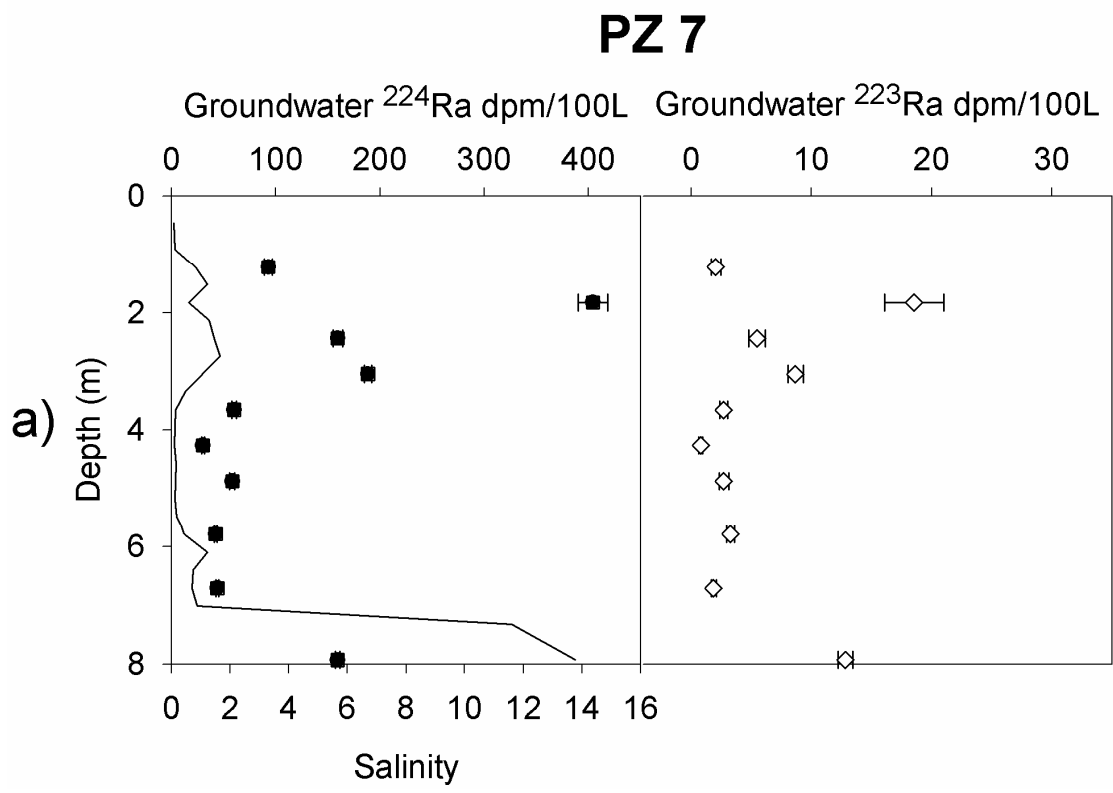


Figure 2a

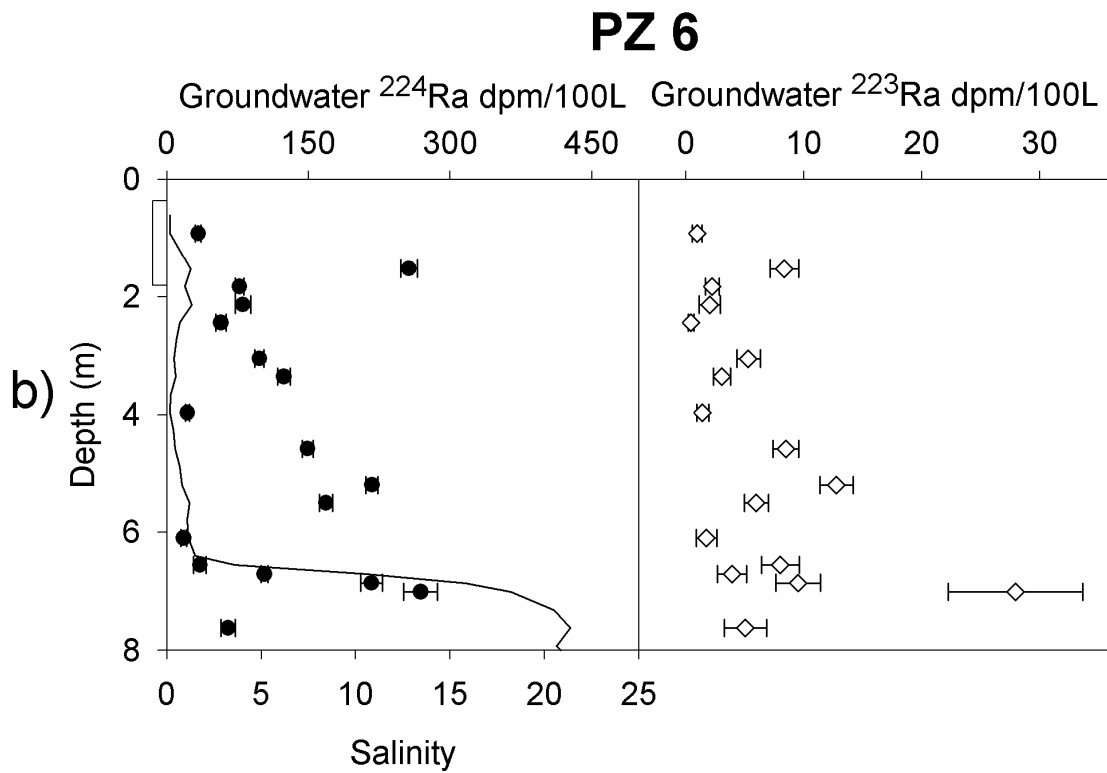


Figure 2b

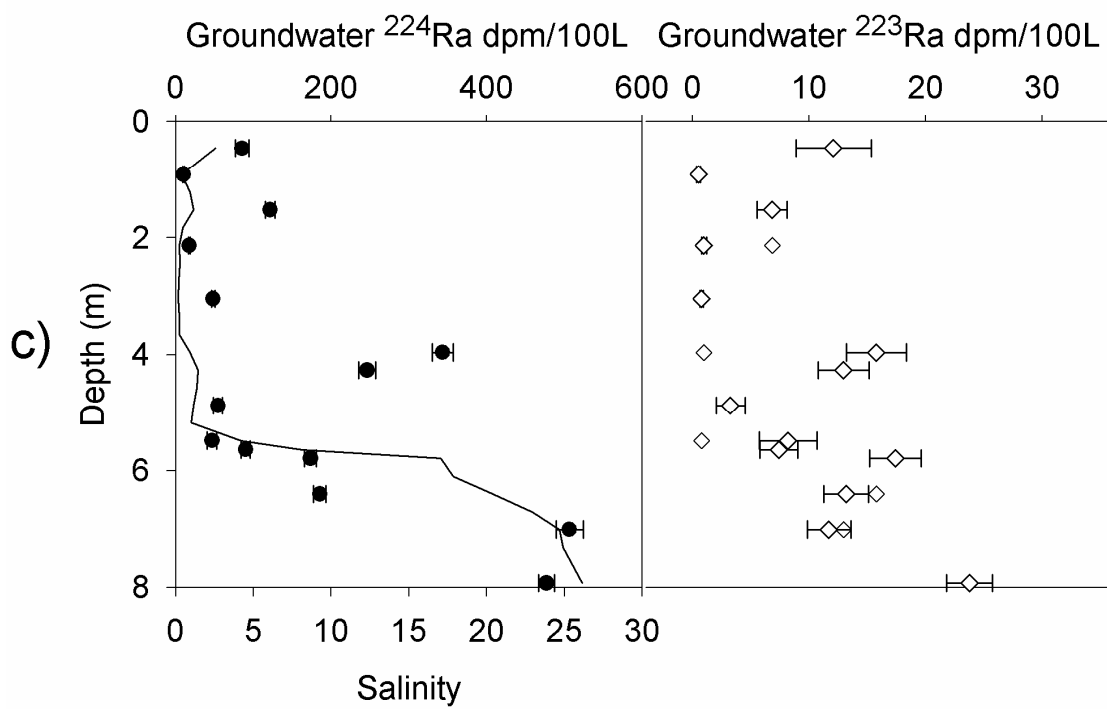
**PZ 11**

Figure 2c

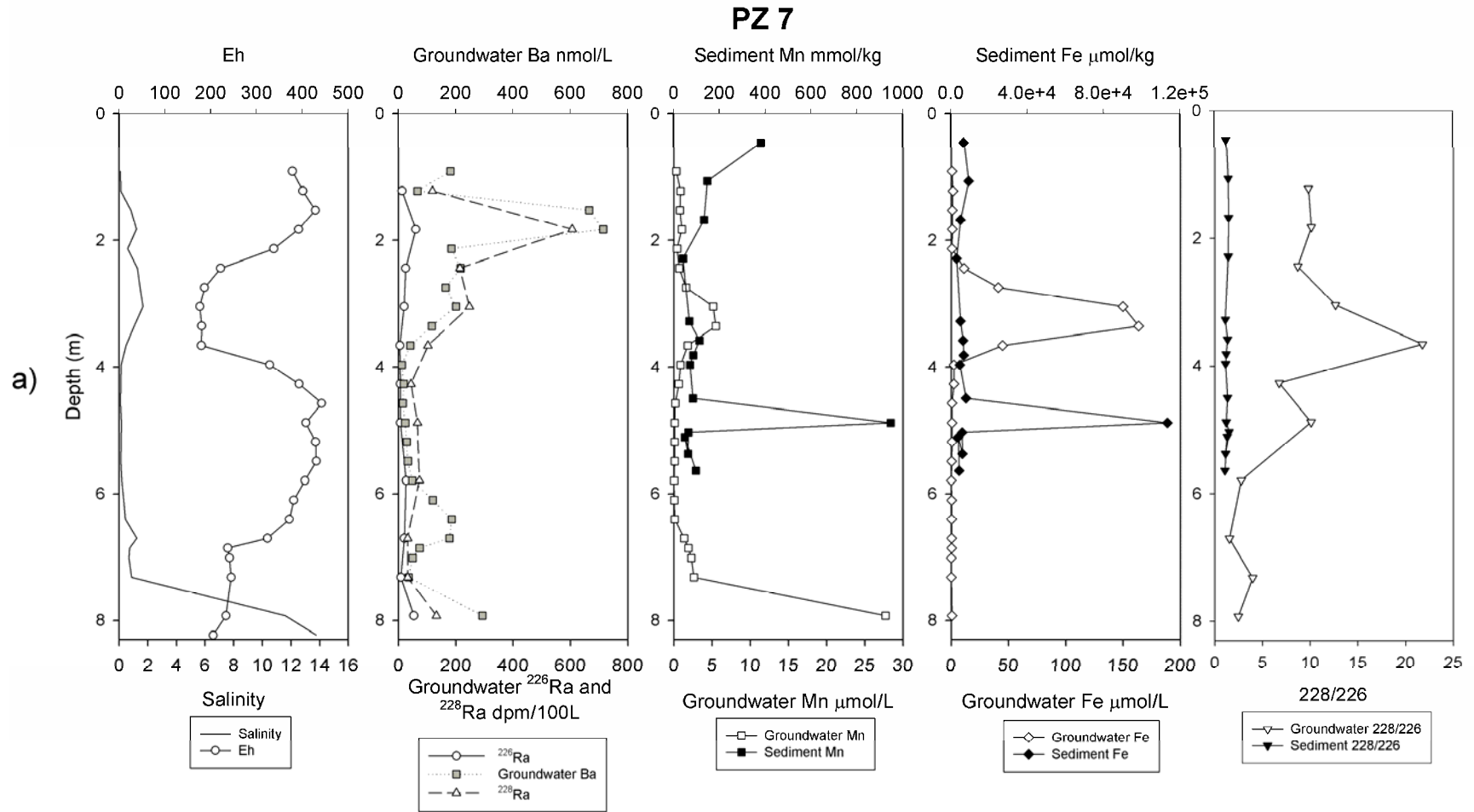


Figure 3a

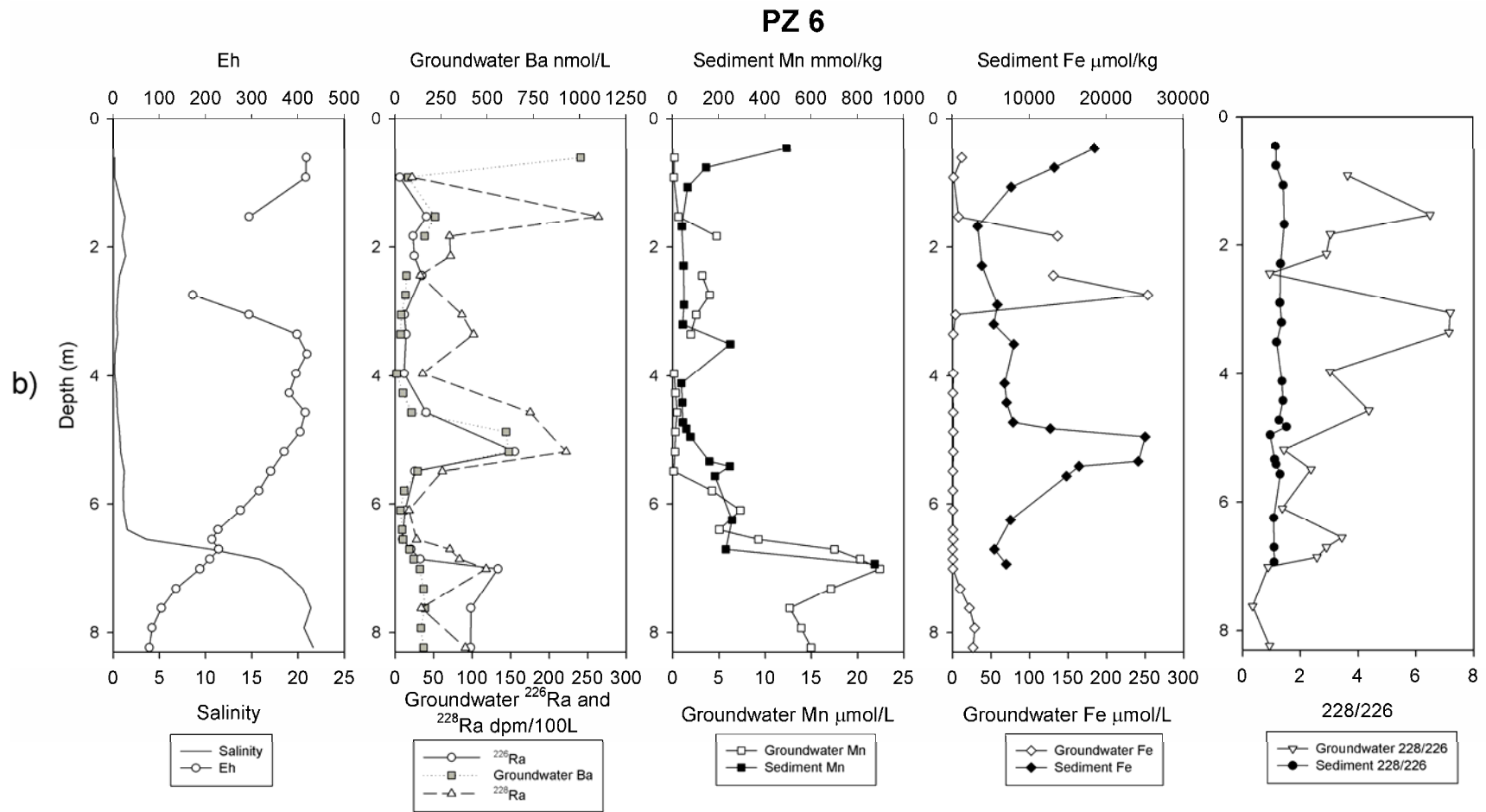


Figure 3b

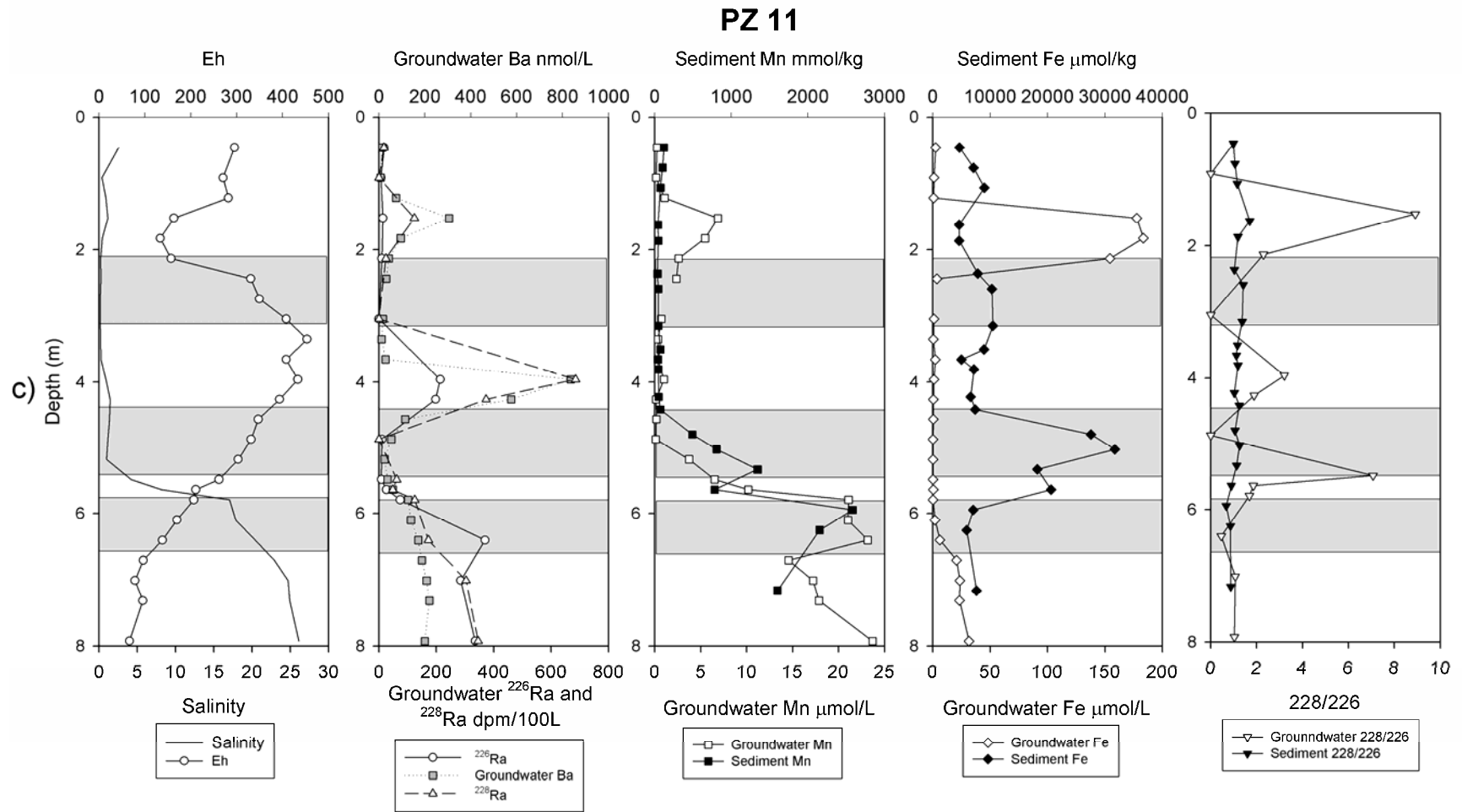


Figure 3c

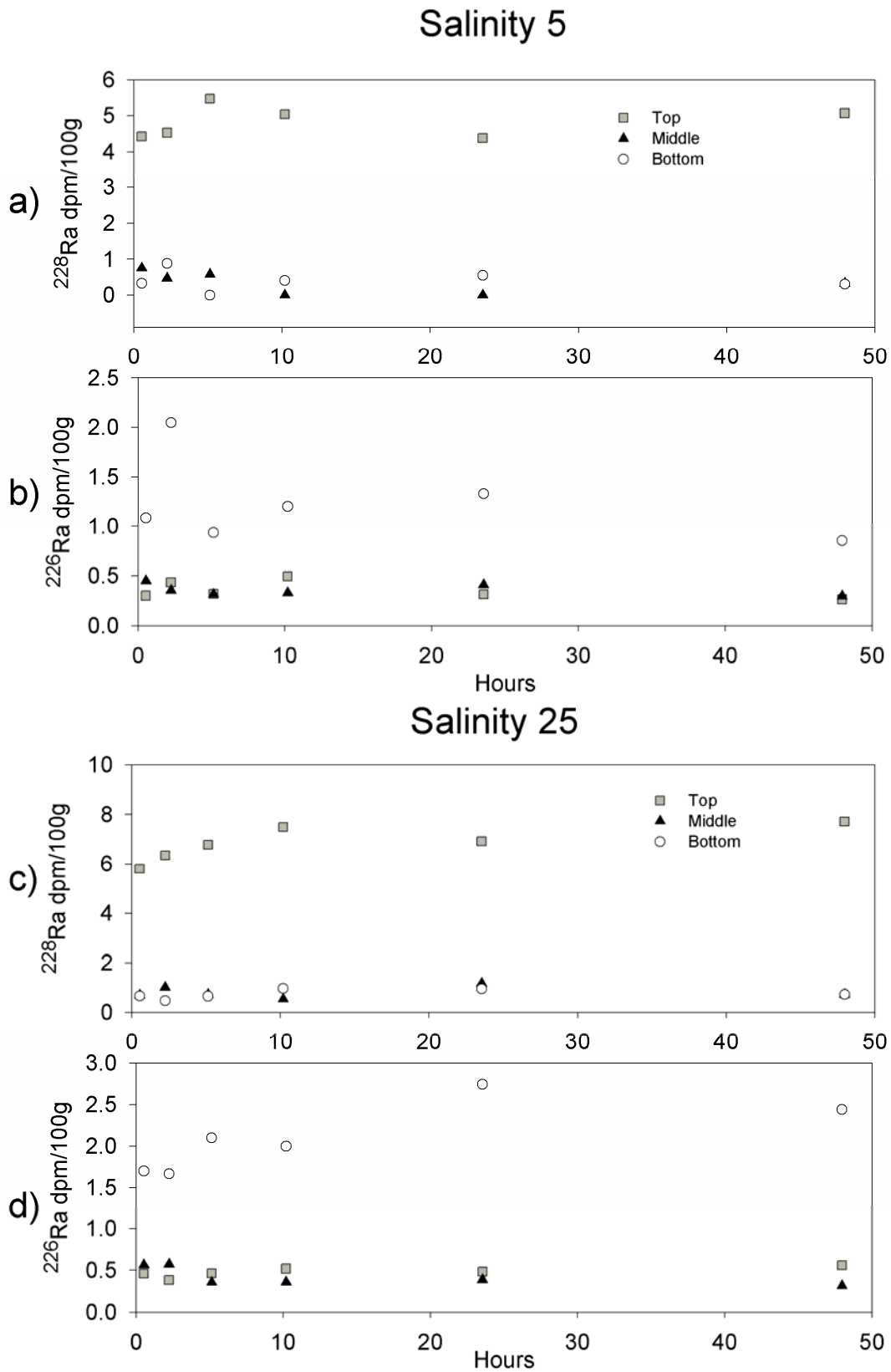
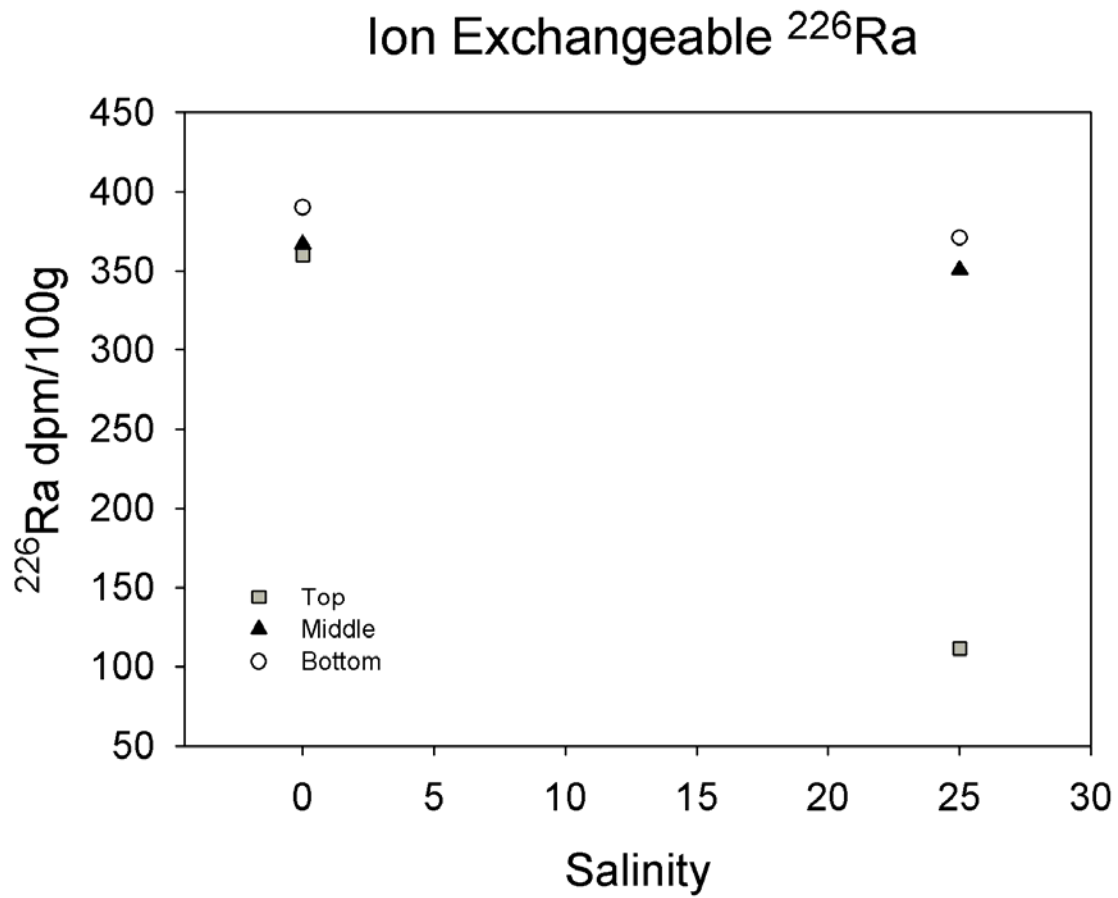


Figure 4



**Figure 5**

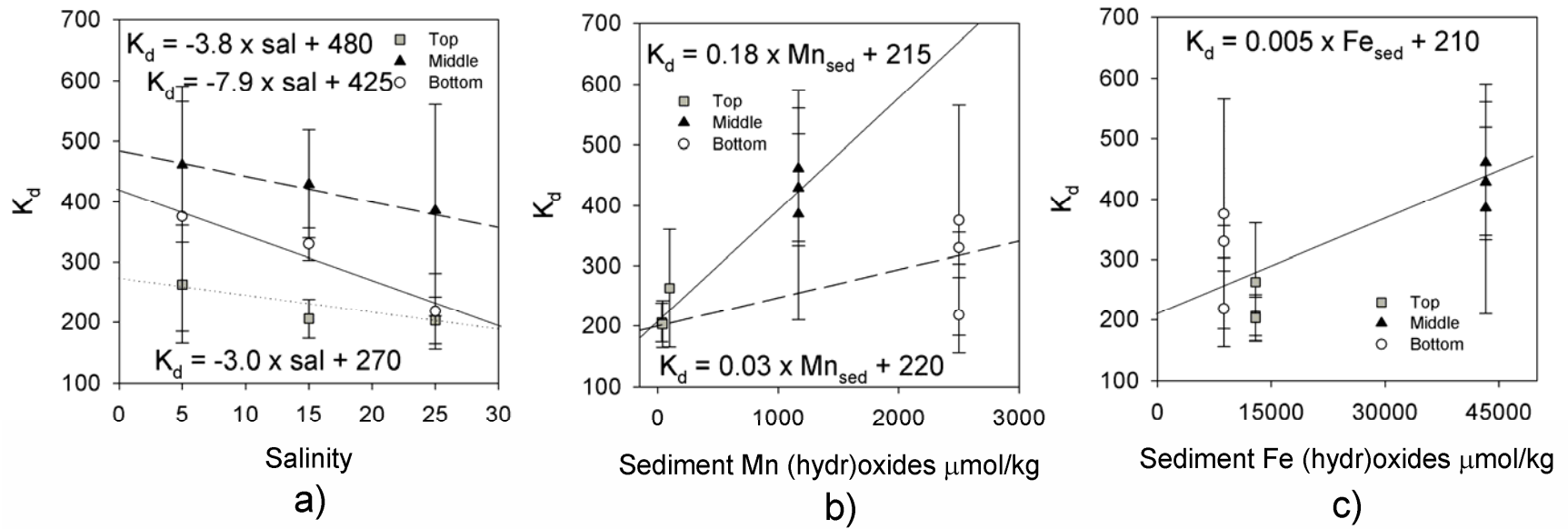


Figure 6 a-c

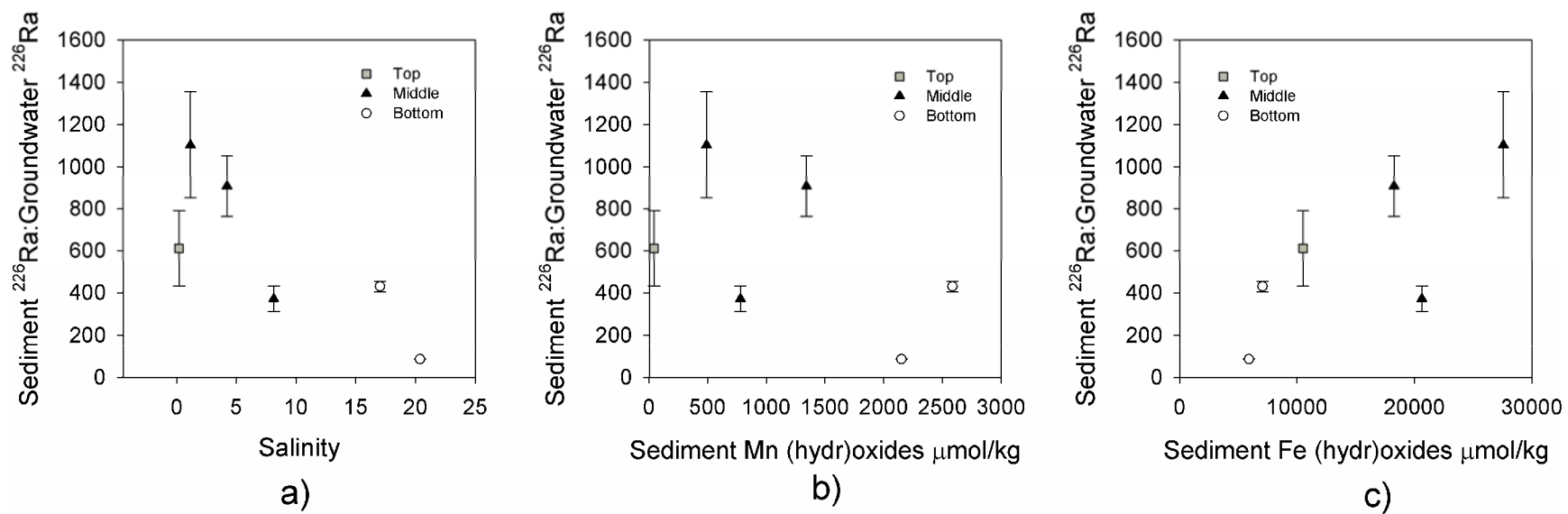


Figure 7 a-c

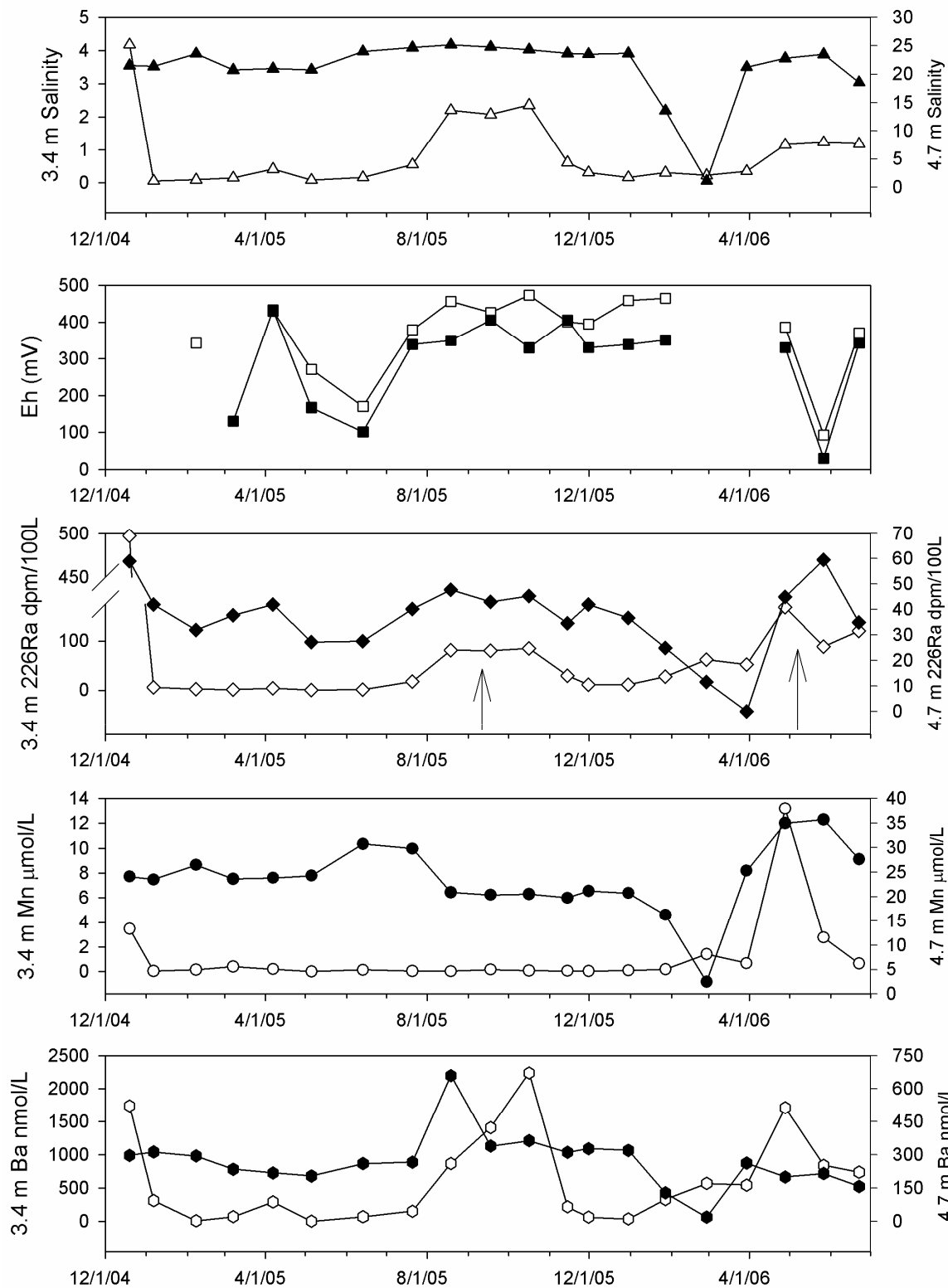


Figure 8